Organic &
Biomolecular
Chemistry

www.rsc.org/obc

Volume 1 | Number 1 | Jan 2013 | Pages 1–100

ROYAL SOCIETY
OF CHEMISTRY

This is an *Accepted Manuscript*, which has been through the Royal Society of Chemistry peer review process and has been accepted for publication.

Accepted Manuscripts are published online shortly after acceptance, before technical editing, formatting and proof reading. Using this free service, authors can make their results available to the community, in citable form, before we publish the edited article. We will replace this *Accepted Manuscript* with the edited and formatted *Advance Article* as soon as it is available.

You can find more information about *Accepted Manuscripts* in the **Information for Authors**.

Please note that technical editing may introduce minor changes to the text and/or graphics, which may alter content. The journal's standard **Terms & Conditions** and the **Ethical guidelines** still apply. In no event shall the Royal Society of Chemistry be held responsible for any errors or omissions in this *Accepted Manuscript* or any consequences arising from the use of any information it contains.

Validation of a homology model of *Mycobacterium tuberculosis* DXS: Rationalization of observed activities of thiamine derivatives as potent inhibitors of two orthologues of DXS[†]

T. Masini,[a] B. Lacy,[b] L. Monjas,[a] D. Hawksley,[c] A. R. de Voogd,[a] B. Illarionov,[d] A. Iqbal,[c] F. J. Leeper,[c] M. Fischer,[d] M. Kontoyianni[*b] and A. K. H. Hirsch[*a]

[a] Stratingh Institute for Chemistry, University of Groningen, Nijenborgh 7, 9747AG Groningen (The Netherlands). E-mail: a.k.h.hirsch@rug.nl

[b] Department of Pharmaceutical Sciences, School of Pharmacy, Southern Illinois University Edwardsville, Edwardsville, IL 62034. E-mail: mkontoy@siue.edu

[c] Department of Chemistry, University of Cambridge, Lensfield Road, Cambridge, CB2 1EW, (UK).

[d] Hamburg School of Food Science, Institute of Food Chemistry, Grindelallee 117, D-20146, Hamburg (Germany).

ABSTRACT

The enzyme DXS catalyzes the first, rate-limiting step of the 2-*C*-methyl-D-erythritol-4-phosphate (MEP, **1**) pathway using thiamine diphosphate (ThDP) as cofactor; the DXS-catalyzed reaction constitutes also the first step in vitamin B1 and B6 metabolism in bacteria. DXS is the least studied among the enzymes of this pathway in terms of crystallographic information, with only one complete crystal structure deposited in the Protein Data Bank (*Deinococcus radiodurans* DXS, PDB: 2O1X). We synthesized a series of thiamine and ThDP derivatives and tested them for their biochemical activity against two DXS orthologues, namely *D. radiodurans* DXS and *Mycobacterium tuberculosis* DXS. These experimental results, combined with advanced docking studies, guided the development and validation of a homology model of *M. tuberculosis* DXS, which will guide medicinal chemists in rationally designing potential inhibitors for *M. tuberculosis* DXS.

INTRODUCTION

Bacterial and protozoan infections are far from being eradicated from our society, both in developed and developing countries. In particular, tuberculosis and malaria taken together are responsible for the death of approximately two million people every year.[1] The development of new anti-infective agents with new mechanisms of action is particularly important nowadays, given that *Mycobacterium tuberculosis* and *Plasmodium falciparum*, the causative agents of tuberculosis and malaria, respectively, have developed extremely resistant strains against which most of the available drugs are no longer effective.[2]

The 2-*C*-methyl-D-erythritol-4-phosphate (MEP, **1**) pathway for the biosynthesis of the two essential isoprenoid precursors isopentenyl diphosphate (**2**) and dimethylallyl diphosphate (**3**)[3] is a rich source of drug targets for the development of anti-infective agents (Scheme 1a).[4] The fact that humans utilize a completely different metabolic pathway (*i.e.*, the mevalonate pathway) for the biosynthesis of **2** and **3**, renders the enzymes of the MEP pathway important drug targets. 1-Deoxy-D-xylulose-5-phosphate synthase (DXS) catalyzes the first and rate-limiting step of the MEP pathway consisting in the thiamine diphosphate (ThDP)-dependent decarboxylative condensation of pyruvate (**4**) and D-glyceraldehyde 3-phosphate (**5**) to afford 1-deoxy-D-xylulose-5-phosphate (**6**).[5] DXS controls the flux of metabolites at the starting point of the pathway and it was recently shown that it plays an important regulatory role for the whole MEP pathway, having the highest flux-control coefficients together with IspC.[6] Furthermore, DXS is involved both in microbial thiamine (vitamin B_1, **7**)[7] and pyridoxal phosphate (vitamin B_6, **8**) biosynthesis,[8] which renders it a particularly interesting target, with the added benefit of interfering with three essential bacterial biosynthetic pathways at once. Whereas for other enzymes of the MEP pathway, several crystal structures of pathogenic orthologues have been deposited in the RCSB Protein Data Bank (PDB),[4b] just two crystal structures of DXS, from *Deinococcus radiodurans* and *Escherichia coli,* in complex with ThDP have been reported (PDB codes: 2O1X and 2O1S, respectively), where the structure of *E. coli* DXS is incomplete due to in situ proteolysis by a fungal protease during its crystallization.[9] The structure of *D. radiodurans* DXS consists of a tightly associated dimer where the ThDP-binding pocket is located within the same monomer. The amino acid residues defining the ThDP-binding pocket are highly conserved among the DXS enzymes in different organisms (*e.g.*, 38% sequence identity overall and 68% sequence identity in the ThDP-binding pocket of *D. radiodurans* and *M. tuberculosis* DXS).[10]

The high degree of similarity between DXS and human ThDP-dependent enzymes such as transketolase (TK)[11] and the E1 subunit of pyruvate dehydrogenase (PDH)[12] could potentially lead to selectivity problems in the development of inhibitors against DXS (*e.g.*, 20% identity overall, 47% identity in the ThDP-binding pocket of human TK and *M. tuberculosis* DXS).[10] However, DXS has distinctive features compared to other ThDP-dependent enzymes, suggesting that selective inhibition of DXS over other ThDP-dependent enzymes could be possible. Specifically, *D. radiodurans* DXS has an arrangement of domains in which the ThDP-binding site is located within the same monomer9 (and not at the dimer interface as in all the mammalian ThDP-dependent enzymes),[13] a particularly large active site[14] and a unique catalytic mechanism, which requires the formation of a ternary complex with pyruvate and GAP[15] (in contrast, all other ThDP-dependent enzymes follow classical ping-pong kinetics in which the binding of acceptor substrate is preceded by the activation of pyruvate and release of CO_2).[16]
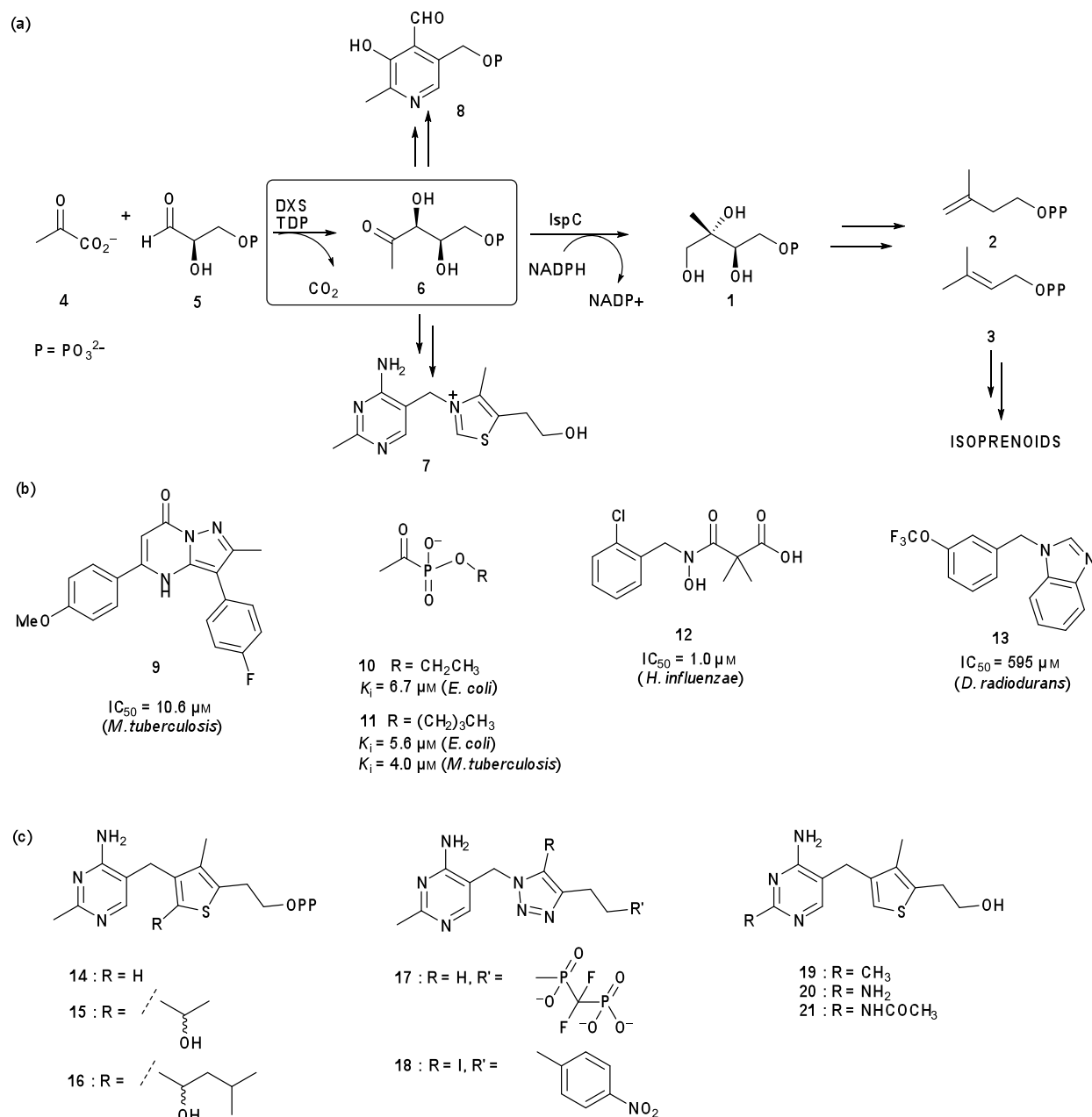
Scheme 1. (a) Schematic representation of the 2-*C*-methyl-D-erythritol-4-phosphate (MEP, **1**) pathway for the synthesis of the universal isoprenoid precursors isopentenyl diphosphate (**2**) and dimethylallyl diphosphate (**3**); **6** is also the branch point for the biosynthesis of vitamin B1 and vitamin B6, as shown. (b) Representative inhibitors of DXS. c) Selection of ThDP- and thiamine-derivatives tested as inhibitors of various ThDP-dependent enzymes.

The lack of structural information available on DXS probably explains the very small number of inhibitors of this enzyme reported so far (*e.g.,* **9−13**, Scheme 1b).[17] Moreover, for most of them, no information about their binding mode is known, rendering the optimization of the inhibitory activities very challenging. Phosphonates **10** and **11** have been developed as substrate (pyruvate)-competitive inhibitors of *E. coli* and *M. tuberculosis* DXS with remarkable selectivity over mammalian ThDP-dependent enzymes,[18] although weak antimicrobial activity was observed probably due to poor cell permeability. The absence of crystal structures of DXS in complex with pyruvate or one of the unnatural bisubstrate analogues is a limiting factor for their further optimization, although a rough identification of the substrate-binding pocket is possible. In fact, certain amino-acid residues of DXS (*D. radiodurans* or *E. coli*) or DXS-homologues (TK and PDH) have been shown by mutagenesis studies to be essential for the catalytic process (referring to *D. radiodurans* DXS: His51,[19] Asp430[20]) while others are thought to be involved in the substrate-recognition process such as Arg480, whereas Tyr395 and His434 have been shown to have minimal impact on the catalytic activity.[9] Nevertheless, the high degree of flexibility associated with the presumed substrate-binding pocket, might render a rational optimization of **10** and **11** challenging. Specifically, the loop defined by residues Lys208 and Ala327 in *D. radiodurans* DXS may move upon ligand binding, resulting in a conformational change.[9]

ThDP- and thiamine derivatives have been widely studied in the past as inhibitors of ThDP-dependent enzymes and riboswitches but none of them has been exploited to date as an inhibitor of DXS.[21] One of the most potent inhibitors of several ThDP-dependent enzymes is 3-deazathiamine diphosphate (**14**, Scheme 1c). The replacement of the charged thiazolium ring of ThDP with the neutral thiophene ring resulted, for instance, in an essentially irreversible inhibition of *Zymomonas mobilis* pyruvate decarboxylase (PDC).[22] Derivatives of **14** substituted

at the C-2 position of the thiophene ring (**15**, **16**, Scheme 1c) closely mimic the intermediates of the ThDP-catalyzed reactions and have been extensively studied to further understand their detailed mechanisms and the conformational changes adopted by the protein during the reaction.[23] Moreover, they have been shown to be potent inhibitors of ThDP-dependent enzymes (e.g., K_i of 0.44 nM (**15**) and 0.17 nM (**16**) for the E1 subunit of branched-chain α-keto acid dehydrogenase).[21]

Diphosphate-free derivatives potentially circumvent cell-penetration issues caused by the presence of the very polar diphosphate moiety, which is also prone to hydrolysis. On the one hand, ThDP-derivatives bearing both charged and neutral diphosphate mimics[24] have been reported (*e.g.*, compounds **17** and **18**, Scheme 1c), which showed very good inhibitory activity (**17**, K_i = 20 pM against *Zymomonas mobilis* PDC; **18**, IC$_{50}$ = 5.33 μM against *E. coli* E1 subunit of PDH).[25]

On the other hand, ThDP-derivatives not bearing any diphosphate mimic have been investigated so as to be diphosphorylated in the cytosol by the enzyme thiamine pyrophosphokinase (TPPK). Deazathiamine (**19**) and its derivatives **20** and **21** display low micromolar affinity (K_d = 18 μM, 2.2 μM and 1.1 μM, respectively) for TK.[26] Despite retaining TPPK activity, their activity against TK in the cell-based assay decreased compared to the charged thiamine mimics, probably due to the fact.

Given the lack of structural information regarding *M. tuberculosis* DXS, we initiated a structure-based effort by constructing a homology model. Subsequently, we docked a series of ThDP and thiamine derivatives into the homology model of *M. tuberculosis* DXS and the crystal structure of *D. radiodurans* DXS in an effort to validate the model-built structure. By doing so, we were

able to rationalize the activity differences observed for these new inhibitors of DXS against the two orthologues.that these scaffolds are not recognized by thiamine transporters.

RESULTS AND DISCUSSION

M. tuberculosis DXS model-building

Model building is based on the principle that orthologues with similar primary sequences are expected to have similar structures. Consequently, higher homology between the target and template sequences would be expected to result in a more accurate model of the target protein. We employed NCBI's BLAST search (http://blast.ncbi.nlm.nih.gov/Blast.cgi) in order to identify the most appropriate template(s) for our comparative modeling experiments.[27] Selection criteria included percent identity and similarity.

We generated models using the ClustalW alignment of the template, followed by refinement with energy minimization (see Experimental Section). We opted against subsequent constrained dynamics and an implicit solvent model because the model-built structure seemed to satisfy our feasibility criteria (see explanation below). To assess the models we employed DOPE[28] and Verify-3D [29] scores, and Ramachandran plot analyses. DOPE corresponds to the energy accounting for the relative stability of a conformation with respect to other conformations of the same protein. Verify-3D scores assess whether a residue is in the desired 3D environment, and is mostly driven by packing; thus hydrophobic residues on a protein's surface and polar residues in the core are penalized by having lower scores. Consequently, a model region with a low score, or lower than the expected values, should be carefully examined. The quality of 'a' model can often be improved by adjusting the sequence alignments.

The *M. tuberculosis* DXS homology model has a low DOPE score (−68.21), which in turn is indicative of small errors in the conformational energy of atoms between different residues. Furthermore, the closer the Verify-3D score is to the expected high score, the more optimal the residue compatibility. The model's Verify-3D score of 264.65 is close to the expected high score (expected Verify-3D scores range from 287.92 to 129.56) and within the range of the 3D profile scoring function. It should be noted that the expected 3D scores are based on a statistical analysis of high-resolution structures in the PDB. We also analyzed the stereochemical quality of the protein side chains in the model. Toward that goal, we generated Ramachandran plots in order to highlight regions with unusual geometry and provide an overall assessment of the quality of the structure (Figure S3 in the ESI†). It can be seen that very few residues are in the disfavored quadrant, with most of them being glycine residues. Therefore, the scoring functions along with the packing-quality analyses suggest that the model-built *M. tuberculosis* DXS structure is viable with most residues placed in a physically acceptable environment after refinement.

Comparison of the ThDP- and substrate-binding pockets in *D. radiodurans* DXS and *M. tuberculosis* DXS

As mentioned above, there is a high degree of sequence identity in the ThDP-binding pocket of *D. radiodurans* and *M. tuberculosis* DXS (70% identity in the ThDP binding pocket; 54% similarity overall, 35% identity overall). A detailed comparison of the amino acids lining the ThDP- and substrate-binding pockets (Table 1), reveals the high degree of similarity. Especially in the subpocket hosting the aminopyrimidine ring of ThDP, all the amino acids are conserved. In the diphosphate-binding pocket, where most of the interactions rely on hydrogen bonds with

the protein backbone, a strict conservation might not be needed to preserve the strength of the binding. It is particularly interesting that the small subpocket hosting the thiazolium ring of ThDP shows the lowest degree of similarity. Residues Val80 and Ile187 in *D. radiodurans* DXS are engaged in hydrophobic interactions with the thiazolium ring, keeping it in place together with Ile371. In *M. tuberculosis* DXS, the hydrophobic contacts are fewer due to the replacement of Val80 and Ile187 by the more hydrophilic Thr69 and Tyr177, respectively. In particular, Tyr177 is involved in a favorable intramolecular edge-to-face π-stacking interaction with His296 and, as a result, it lies too far from the thiazolium ring for interacting with it (Figure S4 in the ESI†).

Table 1. Comparison of the amino acids in the ThDP-binding pocket of *D. radiodurans* DXS (PDB code: 2O1X) and *M. tuberculosis* DXS (homology model)	
***D. radiodurans* DXS (2O1X)** [a]	***M. tuberculosis* DXS (homology model)**
ThDP-binding pocket	
Aminopyrimidine-binding pocket	
Gly123 (C=O)[b]	Ser112
His124	**His113**
Ala125	**Ala114**
Glu373	**Glu365**
Phe398	**Phe390**
Arg401	**Arg393**
Thiazolium-binding pocket	
Val80	*Thr69*
Ser186	**Ser176**
Ile187	*Tyr177*
Met349	**Met341**
Ile371	**Ile363**
His304	**His296**
Diphosphate-binding pocket	
Ser54	*Pro43*
His82	**His71**
Asp154	**Asp144**

Gly155	Gly145
Ser156 (N-H)[(b)]	Ala146
Asn183	**Asn173**
Met185 (C=O)[(b)]	Arg175
Substrate-binding pocket	
His51	**His40**
Tyr395	**Tyr387**
Asp430	**Asp422**
Residues in proximity of the substrate-binding pocket	
Lys101[(c)]	Arg90
His304	**His296**
Arg423	**Arg415**
Arg480[(c)]	Lys473
(a) Amino-acid residues, which are conserved, are shown in bold, whereas non conserved amino-acid residues are shown in italics. (b) Non conserved amino-acid residues, which are involved in binding ThDP using the protein backbone. (c) Non conserved amino-acid residues, with a high degree of similarity in terms of polarity.	

Synthesis and biological evaluation of ThDP derivatives

First, we decided to synthesize two very closely related derivatives of ThDP, 3-deazathiamine diphosphate (**14**) and racemic 2-(1-hydroxyethyl) thiamine diphosphate (**15**). We synthesized **14** according to a literature procedure,[30] whereas we synthesized **15** starting from deazathiamine (**19**, synthesized according to a literature procedure).[30] **19** was bis acylated using standard Friedel − Crafts conditions to yield **22**, which was subsequently hydrolyzed affording **23**. After introduction of a tosylate moiety on the hydroxyl group of the ethylene linker (compound **24**), reduction of the keto group of **24** with NaBH$_4$ yielded the racemic intermediate **25**. Introduction of the diphosphate moiety was performed in the very last step affording the racemic target molecule **15** (Scheme 2a).

Whereas **14** displays nanomolar IC$_{50}$ values both against *D. radiodurans* DXS and *M. tuberculosis* DXS (**14**: IC$_{50}$ = 0.034 ± 0.006 μM, *D. radiodurans* DXS; IC$_{50}$ = 0.74 ± 0.13 μM,

M. tuberculosis DXS) biochemical evaluation of **15** resulted in a single-digit micromolar IC_{50}

value against *M. tuberculosis* DXS ($IC_{50} = 1.4 \pm 0.1$ μM) but in an IC_{50} of 434 ± 51 μM against

D. radiodurans DXS (Table 2). It should be noted that neither **14** nor **15** represent good lead

compounds given that they feature diphosphate moieties and are therefore not drug-like.
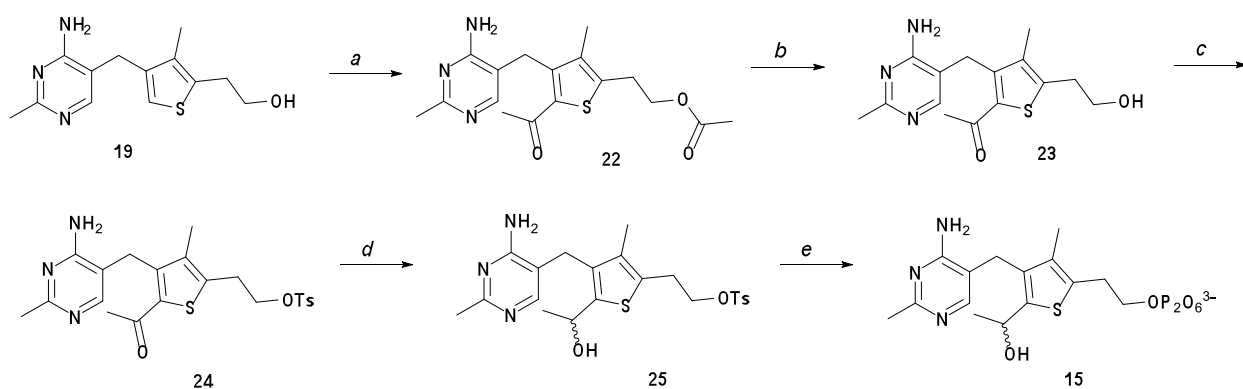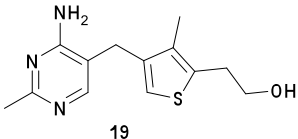

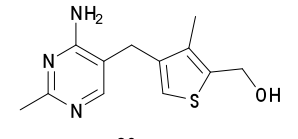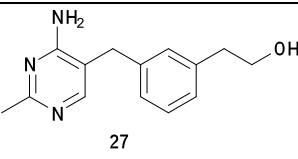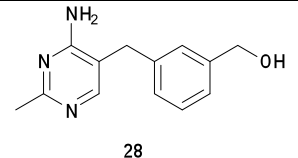**Scheme 2.** Synthesis of the thiamine diphosphate (ThDP) derivative **15**.

Reagents and conditions for the synthesis of **15**: AlCl₃, acetyl chloride, dichloroethane, rt, 2 h,

88%; (b) K₂CO₃, MeOH, rt, 1 h, 97%; (c) TsCl, pyridine, −5 °C, 1 h, 86%; (d) NaBH₄, MeOH,

rt, 3 h, 82%; (e) $(Bu_4N^+)_3HPO_2O_6^{3-}$, acetonitrile, 4 °C, 8 h, 61%.

Given the high degree of similarity between the primary sequence of *D. radiodurans* DXS and

M. tuberculosis DXS, it is remarkable that the inhibitory potency of the same molecule can differ

so much between two orthologues.

Not surprisingly, biochemical evaluation of **19**, not bearing any diphosphate moiety, resulted in a decrease in inhibitory potency against *D. radiodurans* DXS (IC_{50} = 430 ± 68 μM) while no activity at all was observed against *M. tuberculosis* DXS.

Compound **26** (synthesized according to a literature procedure)[31] where the hydroxyethyl substituent of **19** is substituted by a hydroxymethyl substituent, shows a slightly higher IC_{50} value than **19** against *D. radiodurans* DXS (IC_{50} = 526 ± 52 μM) and no activity against *M. tuberculosis* DXS. In our previous work, where we validated the binding mode of **19** to *D. radiodurans* DXS in solution by saturation-transfer difference (**S**TD), **t**rNOE and interligand NOE for pharmacophore mapping (**I**NPHARMA) (STI)-NMR spectroscopy,[10] we showed that **19** binds competitively to ThDP and that its hydroxyl group of **19** is engaged in a strong hydrogen-bonding interaction with the side chain of His82. From our molecular-modeling studies, performed with the software MOLOC,[32] the hydrogen-bonding interaction with His82 is lost when shortening the linker, and the newly formed hydrogen-bonding interaction with Ser186, causes a certain degree of intramolecular strain, which presumably explains the drop in inhibitory activity (Figure S1 in the ESI†). On the other hand, **26** is an interesting scaffold to be decorated with bulkier diphosphate-mimics, for which the ethylene linker of **19** is too long. As we will discuss in the next section, there is a remarkable polarity difference in the pocket hosting the thiazolium ring of ThDP between the two orthologues. To explore the possibility of gaining in affinity by increasing the hydrophobic contacts of the ligand with the enzyme, we synthesized compound **27** conveniently in three steps, according to a literature procedure.[31] Whereas we found **27** to be inactive against *M. tuberculosis* DXS, its inhibitory potency with respect to *D. radiodurans* DXS (IC_{50} = 109 ± 16 μM) increased remarkably compared to **19**, proving that an increase in hydrophobic contacts in this subpocket can lead to a more potent inhibitor.

Shortening the ethylene linker of **27** (compound **28**, Table 2) resulted in a decrease in biological activity (IC_{50} = 255 ± 23 µM), presumably due to the formation of a weaker hydrogen-bonding interaction with His304 (Figure S2 in the ESI†). Like **26**, compound **28** could be a good scaffold to explore different and bulkier diphosphate mimics.

Table 2. Derivatives of ThDP synthesized and tested against *D. radiodurans* DXS and *M. tuberculosis* DXS

	IC_{50} (µM)[a]	
	D. radiodurans DXS	*M.tuberculosis* DXS
14[b]	0.034 ± 0.006	0.74 ± 0.13
15[b]	434 ± 51	1.4 ± 0.1
19	430 ± 68	> 2000
26	526 ± 52	> 2000
27	109 ± 16	> 2000
28	255 ± 23	> 2000

[a] IC_{50} values were determined using a photometric assay using the program Dynafit.[33] Full details of the biochemical assay conditions are provided in the Experimental part; [b] The compounds were isolated and tested as a 1:1 mixture of the compound and ammonium tosylate.

Ligand Docking

We recently studied and validated the binding modes of compounds **19** (Table 2) and **29** (Figure 1B) within *D. radiodurans* DXS by STI-NMR spectroscopy.[10, 34] In an effort to assess Glide's[35]

14

ability to reproduce the above experimental binding modes, we first docked **19** and **29** into the

crystal structure of *D. radiodurans* DXS (PDB code: 2O1X). Figure 1 depicts the binding modes

of compounds **19** and **29** observed by NMR (colored by element) superimposed onto the docked

poses into 2O1X (red). It should be noted that both predicted solutions are top-ranked. We and

others have reported that ranking efficacy is not always optimal, and thus identification of

plausible binding modes should not rely solely on scoring.[36] It is best to examine a certain range

of poses with an arbitrary energetic cutoff from the computed global minimum. The set of poses

is examined in terms of the number and type of non-covalent interactions with surrounding

residues in the pocket as well as their geometrical preferences and local environment. In turn,

this increases confidence in the ability of the method to reproduce reality, and enables calibration

of presumed global minima against docking scores. It was reaffirming that the top-ranked

solutions are almost perfectly overlayed, with the exception of the tilted imidazole ring in

compound **29**; however, all interactions with the binding pocket are reproduced. In a further

effort to validate the docking algorithm, we performed a structural alignment of 2O1X,

complexed with compounds **19** and **29**, and our newly constructed *M. tuberculosis* DXS model.


A.   **B.**
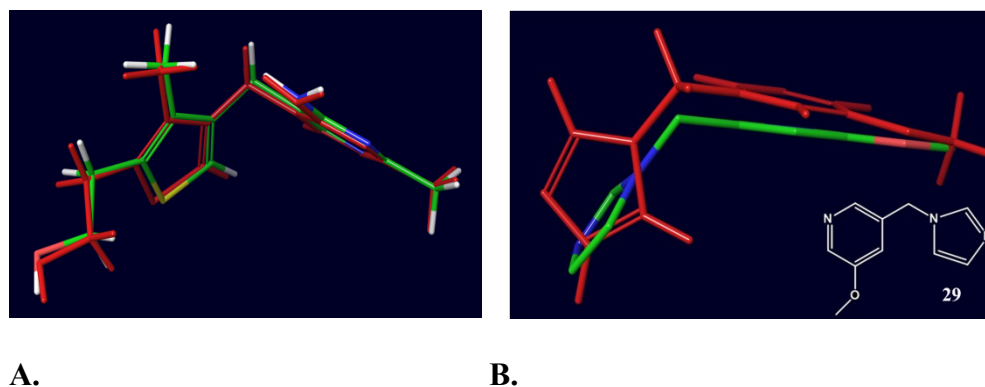
Figure 1. (A) Binding mode of compound **19** validated by STI-NMR spectroscopy (colored by-

element) superimposed onto the predicted docked pose (red). **(B)** Overlay of the binding mode of

compound **29** (colored by-element) validated by STI-NMR spectroscopy and our predicted docked pose (red).

The rationale was that we could *"infer"* the binding interactions of **19** and **29** with the model-built *M. tuberculosis* DXS based on the topology of these compounds within 2O1X. Subsequently, we docked the ligands into the model and compared the resultant predicted solutions against the "inferred" binding modes. It appears that the top and third-ranked solutions (for **29** and **19**, respectively) correspond to poses, which reproduce all interactions seen in the "inferred" orientations (data not shown). Therefore, Glide was able to reproduce experimental binding modes, thus enabling us to further explore docking solutions of the synthetic targets presented herein.

In order to understand differences in activities, we compared binding modes of compounds **14** and **15** into *M. tuberculosis* DXS and *D. radiodurans* DXS employing docking experiments. As can be seen in Table 2, these molecules are active in both targets, albeit with different selectivities. Predicted binding of **15** into *D. radiodurans* DXS resulted in a mode very similar to the native cofactor, with the only exception that the pyrimidine-amino moiety is making different interactions (Figure 2). The amine substituent is observed to make a weak hydrogen bond with the sulfur atom of Met349 and the backbone carbonyl oxygen of Pro347, whereas in the crystal structure of *D. radiodurans* DXS it interacts with the backbone carbonyl oxygen atom of Gly123 and backbone amine hydrogen atom of Ala125. In both complexes, the methionine–aryl interaction is maintained, as well as interactions observed in the *D. radiodurans* DXS crystal structure.

A.
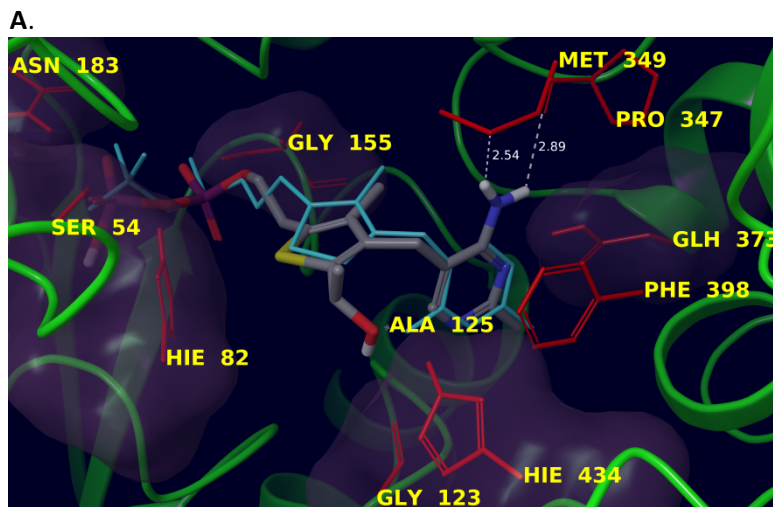
B.
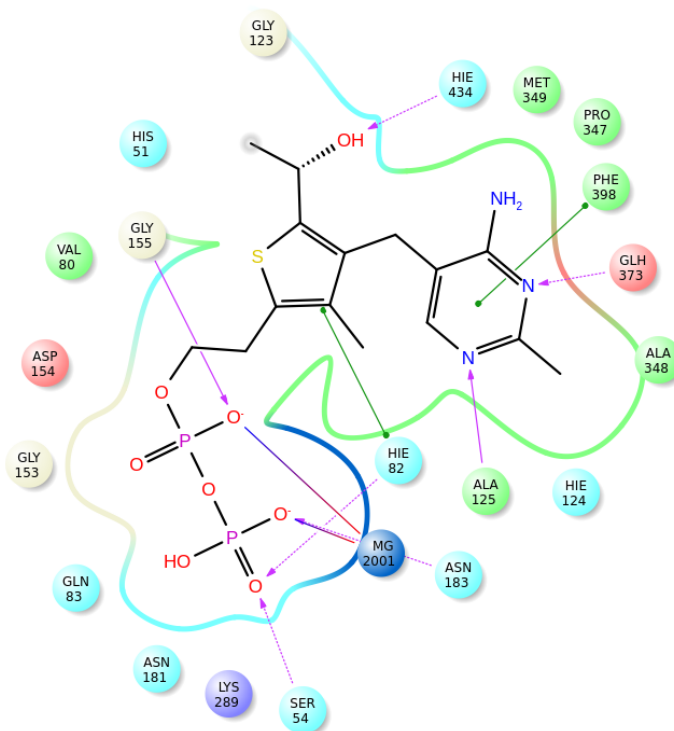
Figure 2. (A) Compound **15** in *D. radiodurans* DXS (colored by element) superimposed with the native cofactor (light blue) in the crystal structure. HIE and GLH correspond to protonation states of His (with H at ε-position) and Glu, respectively, throughout the whole text; (B) Schematic depiction of the *D. radiodurans* DXS−**15** complex within the binding pocket. Pink arrows denote hydrogen-bonding to backbone (solid lines) or side chains (dotted), while straight lines (green) represent π-stacking interactions.

Docking of compound **15** into the model-built M. *tuberculosis* DXS (Figures 3A, 3C) predicts the ligand to form a strong hydrogen bond with Tyr98 (2.21 Å), whereas the thiophenyl ring and the pyrimidine nitrogen atom hydrogen bonds with His71 (2.96 Å) and Tyr387 (3.15 Å), respectively. Similarly to 2O1X, the interactions between the diphosphate moiety and Asn173 (backbone), Asn171, Asp144, Gly145, and Ala146 (backbone) are strong with some of them being bidentate (backbone NH of Asn173 and Asp144). Finally, π-stacking interactions are observed between His426, Tyr387, Phe390 and the pyrimidinyl ring; aromatic–aromatic interactions between His71, His296 and the thiophenyl ring. Furthermore, the observed binding mode has the best emodel score (results not shown), thus pointing to a rather favorable target−ligand complex. Consequently, stabilizing interactions along with favorable energetics may provide an explanation for the higher activity of **15** against *M. tuberculosis* over *D. radiodurans* DXS.
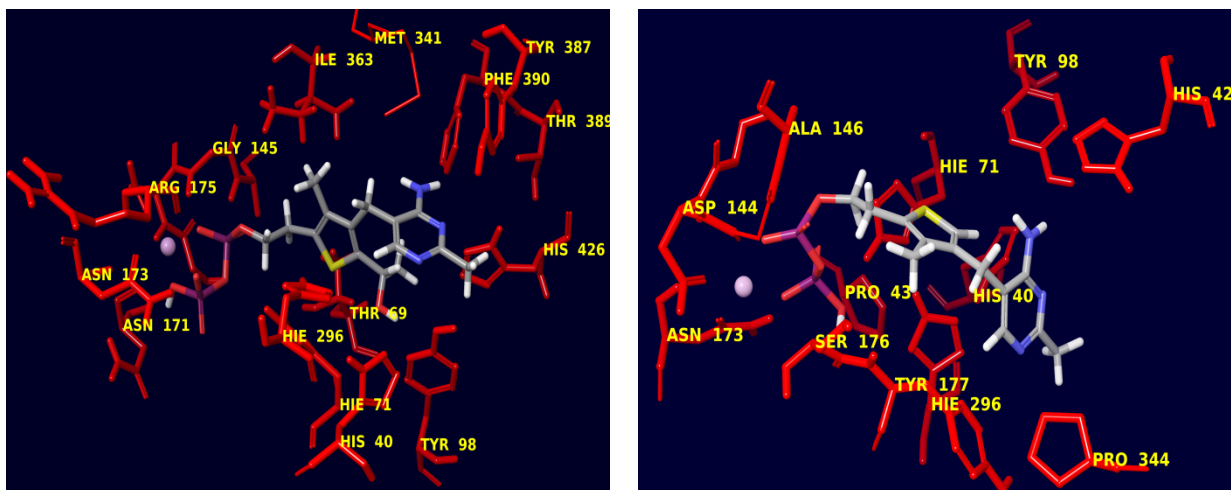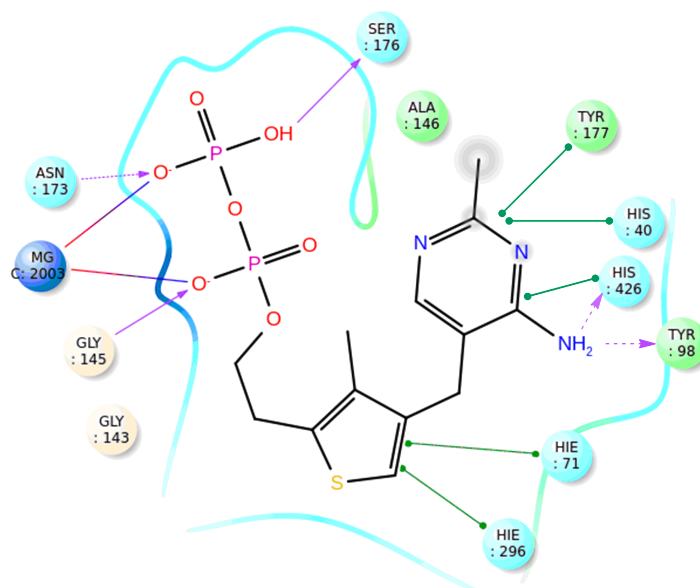
A.

B.
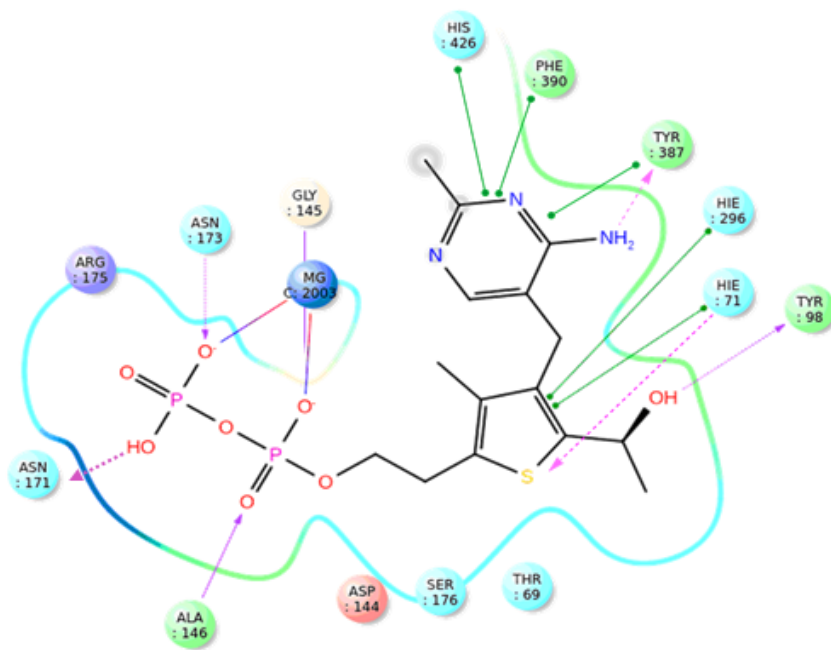
C.

D.

Figure 3. Observed interactions of compounds **15** (A) and **14** (B) in the *M. tuberculosis* model-built structure. Magnesium is shown as a purple sphere. The 2D ligand-interaction diagrams of **15** and **14** are depicted in panels C and D, respectively. Solid pink designates hydrogen-bonds to the protein backbone, dotted pink corresponds to hydrogen-bonds with residue side-chains, and green lines designate π-stacking interactions. Ala146 is not shown in panel A due to its location relative to the residues forming interactions that would in turn hinder its visibility.

In contrast, compound **14** was found to have a higher affinity toward *D. radiodurans* DXS than *M. tuberculosis* DXS. In comparing the binding mode of this structure to that of the natural cofactor in 2O1X, only the thiophenyl ring seems to be oriented differently, thus leading to one interaction being lost, that is with His82 (results not shown). It should be noted that this is the top-scored pose, contrary to the fifth-ranked binding mode, which may have the thiophenyl ring overlapping with that from the ligand of the crystal structure 2O1X. Nevertheless, some interactions of the diphosphate moiety are lost. Thus, we selected the top-ranked pose for subsequent evaluation. Docking into the *M. tuberculosis* DXS model resulted in a second-ranked

pose, based on the number, type and strength of favorable interactions (Figures 3B, 3D). The pyrimidine-amino group is forming hydrogen bonds with His426 (3.49 Å) and Tyr98 (2.70 Å), and the sulfur is interacting with His71. π-Stacking interactions are observed with His426, His40, Tyr177 and Tyr98. Also, aromatic-aromatic interactions are seen between His71 and His296 and the thiophenyl ring. Finally, Ser176, Asn173, Asp144, and Ala146 are coordinating with the magnesium cation and diphosphate moiety.

The fact that **15** has a higher IC_{50} value both against *D. radiodurans* and against *M. tuberculosis* DXS with respect to **14** might arise from the fact that there is a remarkable change in conformation in most of the docked poses of **15** with respect to the original binding mode of ThDP and also with respect to the docked poses of **14**. This is probably due to the fact that the hydroxyethyl substitutent on **15** causes steric clashes with the exocyclic amino group of the aminopyrimidine ring, which is now in a much less favorable conformation than the one of co-crystallized ThDP. By studying the covalent intermediate of the human TK-catalyzed reaction, Tittmann and co-workers already showed how steric clashes with the amino group of the aminopyrimidine ring of the TK-catalyzed reaction intermediate cause pronounced distortion of the reaction intermediate, leading to a reduced barrier to the subsequent step in the TK-catalyzed reaction, and creating an overall efficient process.[37] Our observations might therefore also have implications for the mechanism of the reaction catalyzed by DXS.

Compounds **26, 27** and **28** display inhibitory activity in the three-digit micromolar range against *D. radiodurans* DXS (see Table 2), but no activity was observed against *M. tuberculosis* DXS. In our docking experiments with 2O1X, molecule **26** is predicted to adopt a conformation similar to that of the co-crystallized ligand in 2O1X (Figure 4A and Figure 4C). Specifically, **26** forms bidentate hydrogen-bonding interactions with Gly123 (3.36 Å) and Ala125 (2.94 Å) via its

amine substituent, while the pyrimidine-nitrogen atom interacts strongly with Glu373. Another

hydrogen bond is observed between the pyrimidine-nitrogen atom and the backbone peptide

bond of Ala125, whereas a weak interaction is predicted between His82 and the thiophenyl ring

(3.52 Å). Furthermore, hydrophobic and π-stacking interactions are seen with Phe398, His124,

His82, His304, Met349, and Ala348. Of the poses retrieved after docking of **26** into the *M.*

tuberculosis DXS structure, the second-ranked pose seemed to be the best, amongst others, due

to the larger number of favorable interactions with the receptor (Figure 4B). It should be pointed

out at the outset that the emodel scoring functions between the poses in *D. radiodurans* and

M. tuberculosis DXS differ significantly (−72.519 and −49.945, respectively).

The main differences observed in the conformations and orientations of the ligand within the two

enzymes lies in the pyrimidinyl and thiophenyl rings. Interactions of compound **26** with *M.*

tuberculosis DXS (Figure 4B) include weak hydrogen bonds of Tyr98 (2.22 Å) and His40 (2.98

Å) with the pyrimidine-amino group, and the pyrimidine-nitrogen atom with Tyr98 (3.55 Å).
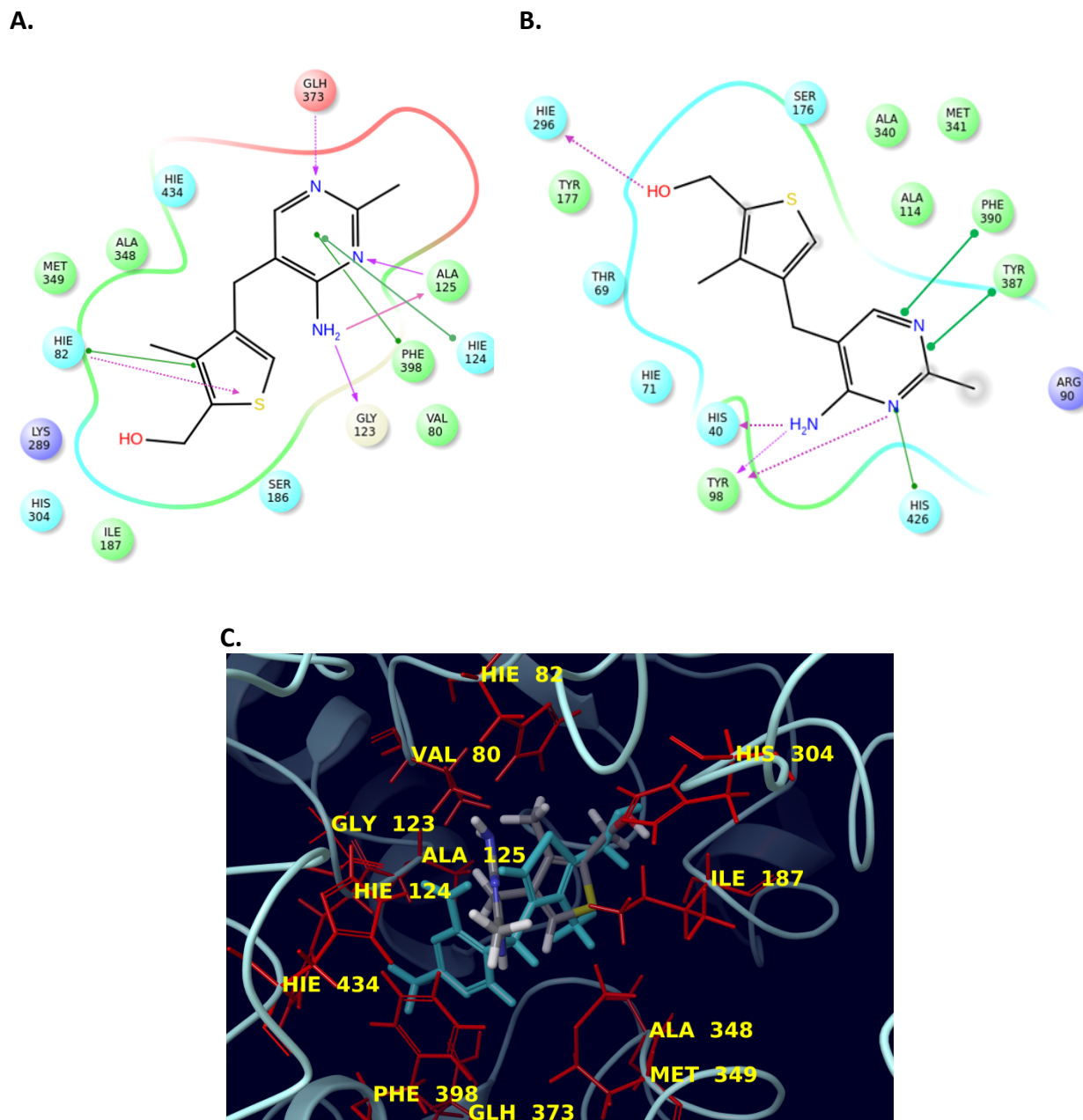
Figure 4. Interactions of compound **26** within the binding pockets of *D. radiodurans* DXS and *M. tuberculosis* DXS (panels (A) and (B), respectively). Arrows denote hydrogen-bonding, while straight lines represent π-stacking interactions. (C) *D. radiodurans* DXS (cyan ribbons) is shown with **26** (cyan) and interacting amino acids (red). The respective pose (colored by element) from *M. tuberculosis* DXS is also depicted based on an overlay of the two enzyme structures.

The hydroxyl group interacts with His296, and the thiophene-sulfur atom with Ser176. Hydrophobic and aromatic interactions are predicted with His71, His426, Phe390, and Tyr387. The energetics and strength of interactions, may account for observed affinity profiles toward the two enzymes.

Compound **27** in *D. radiorurans* DXS displays some very strong contacts with the active-site residues (Figure 5A and 5C). The hydroxyl moiety interacts with His82, Ser54, and Ser186. One of the pyrimidine-nitrogen atoms hydrogen bonds with Glu373, while the other nitrogen atom forms a hydrogen bond with the Ala125 backbone. The amine substituent hydrogen bonds with the Gly123 backbone nitrogen atom. π-Stacking interactions are observed with Phe398, His124, and hydrophobic interactions with Val80 and Ile371. As can be seen in Figure 5B, interactions with *M. tuberculosis* DXS are limited. Contrary to the orientation of the same compound in *D. radiodurans* DXS, in *M. tuberculosis* DXS the pose is flipped (Figure 5C). We reason this is the preferred binding mode (as reflected also by the 7 kcal difference between the top-ranked pose and the one in which the hydroxyl group points toward the metal-coordination site). A strong hydrogen bond between the hydroxyl group and the carbonyl-oxygen atom of Ser112 is observed, and a weaker one between His426 and the same moiety; the pyrimidine-nitrogen atoms hydrogen bond with His71. Finally, the amino substituent is interacting with Asp68. Aromatic−aromatic interactions are observed with His71 and His296.
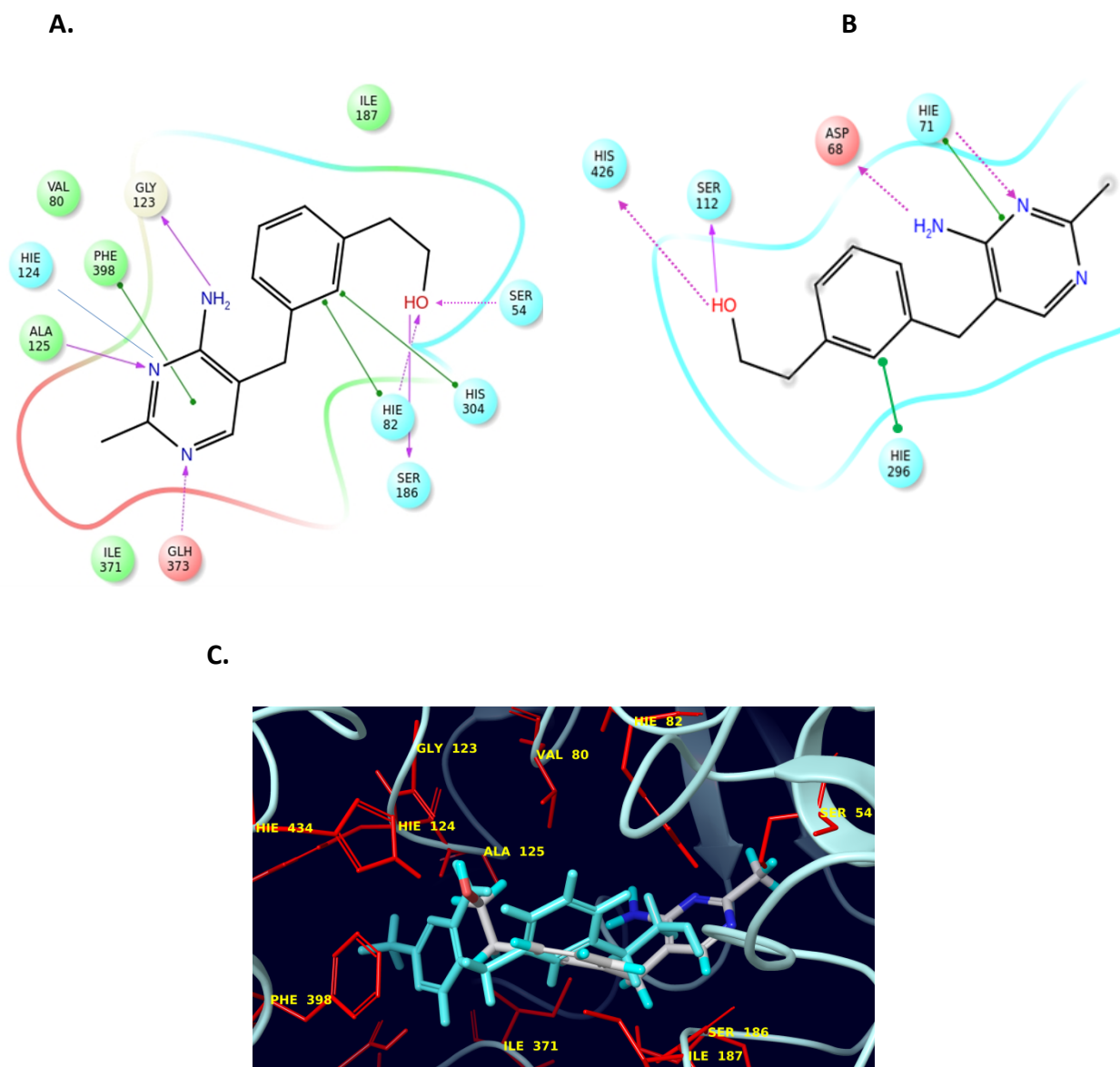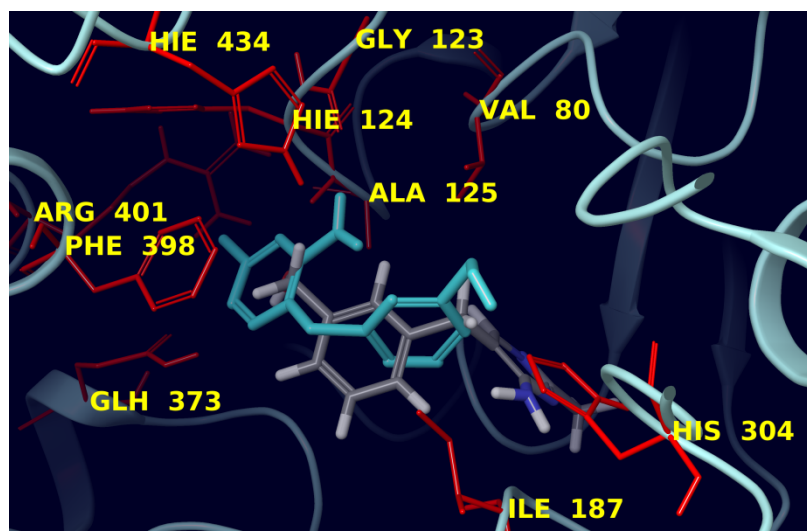
Figure 5. (A) Schematic depiction of the interactions between **27** and *D. radiodurans* DXS; (B) Schematic depiction of the interactions between **27** and the homology model of *M. tuberculosis* DXS. Arrows indicate hydrogen-bonding interactions, whereas straight lines represent π-stacking interactions. (C) Overlay between the ligand bound with *D. radiodurans* DXS (stick representation in cyan) and the predicted binding mode with *M. tuberculosis* DXS (colored by element). Only the *D. radiodurans* DXS is shown in ribbons (cyan).

Compound **28** is inactive toward *M. tuberculosis* DXS, but active against *D. radiodurans* DXS. It can be seen in Figure 6 (panels A and C) that the predicted binding interactions with *D. radiodurans* DXS include hydrogen bonding of its hydroxyl group with His304, its amino-substituent with the backbone carbonyl-oxygen atom of Gly123, and its two pyrimidine nitrogen atoms with the backbone of Ala125 and Glu373 (Figure 6A). π-Stacking interactions are observed with Phe398 and His124. Clearly, the interactions in the predicted binding mode of compound **28** with *M. tuberculosis* DXS appear to be less favorable (Figure 6B). Specifically, a hydrogen bond is formed with Ser176, the exocyclic amino group interacts weakly with His296 and the hydroxyl moiety hydrogen bonds with Ala114's backbone nitrogen atom. Furthermore, there is a noticeable difference in the emodel scores between the predicted poses with the two orthologues, that is −65.735 in 2O1X versus −54.358 in *M. tuberculosis* DXS.

A.

B.
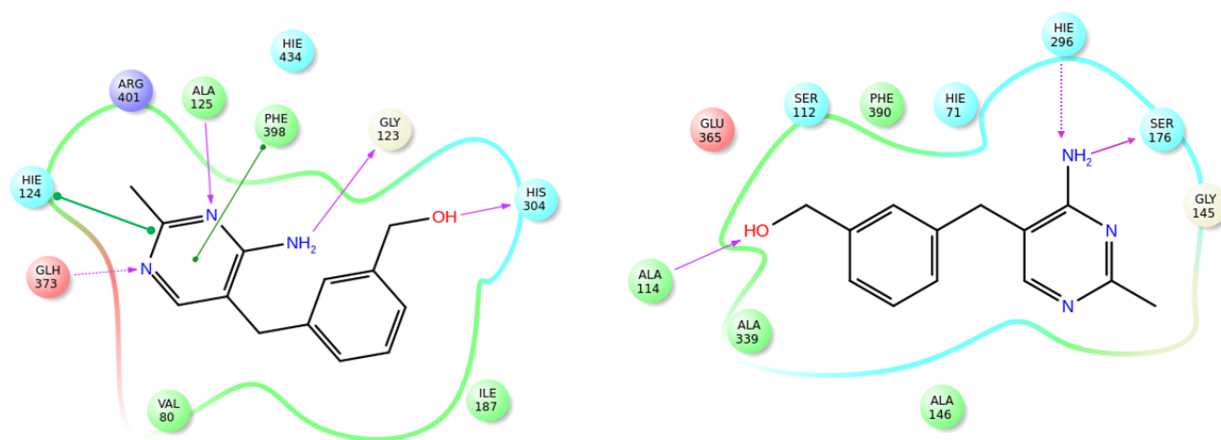
C.

Figure 6. (A) Schematic 2D depiction of the interaction diagram of **28** within *D. radiodurans* DXS; (B) Interactions of **28** within the homology model of *M. tuberculosis* DXS. Arrows indicate hydrogen-bonding, whereas straight lines represent π-stacking interactions. (C) Overlay between the ligand bound with *D. radiodurans* DXS (stick representation in cyan) and its predicted pose with *M. tuberculosis* DXS (colored by element). Only the *D. radiodurans* DXS is shown in ribbons (cyan).

CONCLUSIONS

In summary, we have built a homology model of *M. tuberculosis* DXS and valdiated it by being able to explain observed differences in inhibitory potency of a number of compounds we synthesized against *D. radiodurans* and *M. tuberculosis* DXS employing docking. The compounds we report represent the first ThDP derivatives reported as inhibitors of DXS.

We have also shown that strong stabilizing interactions observed for the high-affinity ligands, in addition to their coordination with the metal cation, can explain experimental data. Binding analyses of all compounds presented herein revealed that either lack of coordination with the metal cation and/or nature and placement of the functional moieties within the ThDP-binding pocket results in predicted poses that lack several binding interactions; this in turn leads to lower binding energies, which correlate with the observed activity differences. The conformational changes we have observed in the thiamine scaffold upon docking the ligands into both orthologues might have important implications for the mechanism of the reaction catalyzed by DXS.

Our results will guide medicinal chemists in rationally designing inhibitors for *M. tuberculosis* DXS. Future structure-based design efforts could take advantage of the SAR we have observed, in particular the subtle differences in sequence that account for substantial differences in activity between the two orthologues studied. The homology model we have constructed could be used to further guide optimization of known inhibitors or the benzene derivatives of thiamine we report herein or any de novo structure-based design project.

EXPERIMENTAL SECTION

Reactions were run using commercially available starting materials (purchased from Aldrich, Acros, Alfa Aesar, Apollo or TCI) without further purification. Yields refer to analytically pure compounds and have not been optimized. All solvents were reagent-grade and, if necessary, dried and distilled prior to use. Column chromatography was performed using silica gel (Silicycle®, Silia*Sep*™ 40‑63 μm or Merck Kieselgel 20, 230-400 mesh). TLC was performed with silica gel 60/Kieselguhr F254. ^{1}H-NMR and ^{13}C-NMR spectra were recorded at 400 MHz on a Bruker AM/DPX 400 spectrometer (400 MHz for ^{1}H, 101 MHz for ^{13}C, 162 MHz for ^{31}P) or a Bruker DPX 500 (500 MHz for ^{1}H, 126 MHz for ^{13}C) at 25 °C. Chemical shifts (δ) are reported relative to the residual solvent peak (CHCl$_3$, ^{1}H = 7.24; ^{13}C = 77.23. CD$_3$OD, ^{1}H = 3.31; ^{13}C = 49.15). Splitting patterns are indicated as (s) singlet, (d) doublet, (t) triplet, (q) quartet, (m) multiplet, (br) broad. High resolution mass spectra were recorded with a Waters LCT Premier TOF mass spectrometer with electrospray and modular Lockspray interface or a Micromass Q-Tof Spectrometer using electron impact (EI) ionization. Melting points were measured with a Buchi melting point B-545. Compounds **14**,[30] **19**,[30] **26**,[31] **27**,[31] and **28**[31] were synthesized according to known literature procedures. The purity of compounds **19**, **26**, **27** and **28** was determined by HPLC (>95%). Compounds **14** and **15** were isolated and tested as a mixture with ammonium tosylate (1:1 molar ratio).

5-(2-Acetoxyethyl)-2-acetyl-3-(4-amino-2-methylpyridin-5-ylmethyl)-4-methylthiophene (22). To a stirred solution of **19** (1.0 g, 3.3 mmol) in dichloroethane (10 mL) at 0 °C under an inert atmosphere was added aluminum trichloride (3.1 g, 22.8 mmol) and acetyl chloride (3.0 g, 38.0 mmol). The reaction mixture was allowed to warm to room temperature, stirred for 2 h and then poured into ice-water (50 mL). The mixture was then neutralized by the addition NaHCO$_3$

and extracted with dichloromethane (3 x 50 mL). Combined organic layers were washed with brine, dried over MgSO$_4$ and concentrated under reduced pressure Purification by column chromatography (SiO$_2$; CHCl$_3$/MeOH, 9:1), afforded **22** as a yellow solid (1.16 g, 88%). mp 260–261 ºC (from toluene). δ_H (400 MHz, CDCl$_3$) 2.057 (3H, s), 2.063 (3H, s), 2.46 (3H, s) and 2.56 (3H, s), 3.08 (2H, t, J = 6.8), 4.10 (2H, s), 4.25 (2H, t, J = 6.8), 5.76 (2H, br s) and 7.95 (1H, s); δ_C (100 MHz, CDCl$_3$) 12.9, 20.9, 25.4, 27.8, 27.9, 30.1, 63.4, 110.5, 133.8, 138.2, 141.2, 143.3, 156.0, 161.9, 165.7, 170.7 and 193.6. HRMS (EI+): calc. for C$_{17}$H$_{21}$N$_3$O$_3$S $[M]^+$ 347.1304, found: 347.1297. Anal. calc. for C$_{17}$H$_{21}$N$_3$O$_3$S: C 58.8, H 6.0, N 11.9, found: C 58.3 H 6.0, N 11.9.

2-Acetyl-3-(4-amino-2-methylpyrimidin-5-ylmethyl)-5-(2-hydroxyethyl)-4-methylthiophene (23). To a stirred solution of **22** (100 mg, 0.29 mmol) in dry methanol (2 mL), K$_2$CO$_3$ (80 mg, 0.58 mmol) was added at room temperature. The reaction mixture was stirred for 1 h before being concentrated under reduced pressure. The resultant residue was taken up in chloroform and washed with water and brine before being dried over MgSO$_4$ and concentrated under reduced pressure to give **23** as a white solid (85 mg, 97%). mp 202–203 °C (from toluene – methanol). δ_H (500 MHz, CD$_3$OD) 2.04 (3 H, s), 2.36 (3 H, s), 2.50 (3 H, s), 3.05 (2 H, t, J = 6.5), 3.78 (2 H, t, J = 6.5), 4.07 (2 H, s) and 7.32 (1 H, s); δ_C (125 MHz, DMSO) 11.8, 25.1, 26.1, 29.6, 31.9, 61.1, 111.0, 133.8, 136.6, 143.2, 143.4, 161.8, 164.3 and 190.7. HRMS (+EI)): calc. for C$_{15}$H$_{29}$N$_3$O$_2$S $[M]^+$ 305.1198, found: 305.1196.

2-Acetyl-3-(4-amino-2-methylpyrimidin-5-ylmethyl)-4-methyl-5-[2-(*p*-toluenesulfonyloxy)-ethyl]thiophene (24). To a solution of **23** (60 mg, 0.20 mmol) in pyridine (1.0 mL) at −5 ºC, *p*-toluenesulphonyl chloride (188 mg, 1.0 mmol) was added

portionwise. The reaction mixture was stirred at −5 ºC for 1 h before being quenched with cold (1 M) aq. HCl (2.0 mL) and neutralized by the addition of $NaHCO_3$. The mixture was extracted with ethyl acetate (3 x 10 mL), and the combined organic layers were washed with a sat. aq. $CuSO_4$ solution, water, and brine, dried over $MgSO_4$, and concentrated under reduced pressure to give **24** as an orange, crystalline solid (76 mg, 86%). mp 149−151 ºC (from $EtOH/H_2O$). δ_H (500 MHz, $CDCl_3$) 1.97 (3 H, s), 2.45 (6 H, s), 2.53 (3 H, s), 3.11 (2 H, t, $J = 6.8$), 4.06 (2 H, s), 4.18 (2 H, t, $J = 6.8$), 5.68 (2 H, br. s), 7.32 (2 H, d, $J = 8.4$), 7.73 (2 H, d, J 8.4) and 7.92 (1 H, s); δ_C (125 MHz, $CDCl_3$) 12.8, 21.6, 25.3, 27.7, 28.3, 30.1, 68.7, 110.4, 127.8 (2C), 129.9 (2C), 132.7, 134.1, 138.6, 139.3, 143.3, 145.0, 155.7, 161.9, 165.8 and 193.4. HRMS (ESI+): calc. for $C_{22}H_{26}N_3O_4S_2$ $[M+H]^+$ 460.1365, found: 460.1341.

3-(4-Amino-2-methylpyrimidin-5-ylmethyl)-2-(1-hydroxyethyl)-4-methyl-5-[2-(*p*-toluenesulfonyloxy)ethyl]thiophene (25). To a stirred solution of **24** (200 mg, 0.44 mmol) in dry methanol (2.0 mL) at 0 ºC under inert atmosphere, sodium borohydride (50 mg, 1.32 mmol) was added portionwise. The reaction mixture was allowed to warm to room temperature, stirred for 3 h and then quenched with ice water (10 mL). The reaction mixture was extracted with ethyl acetate (3.0 x 10 mL) and the combined organic layers were washed with water and brine, dried over $MgSO_4$, and concentrated under reduced pressure to give alcohol **25** as a white, crystalline powder (164 mg, 82%). mp 131−133 ºC (from $EtOH/H_2O$). δ_H (500 MHz, $CDCl_3$) 1.54 (3 H, d, $J = 6.4$), 1.82 (3 H, s), 2.45 (3 H, s), 2.46 (3 H), 3.05 (2 H, t, $J = 6.8$), 3.60 (1 H, d, $J = 16.2$), 3.69 (1 H, d, $J = 16.2$), 4.13 (2 H, t, $J = 6.8$), 5.14 (1 H, q, $J = 6.4$), 5.25 (2 H, br. s), 7.32 (2 H, d, $J = 8.4$), 7.73 (2 H, d, $J = 8.4$) and 7.92 (1 H, s); δ_C (100 MHz, $CDCl_3$) 12.7, 21.6, 25.1, 25.3, 26.6, 28.0, 64.0, 69.5, 111.3, 127.9 (2C), 129.9 (2C), 130.2 132.4, 133.0, 135.0, 141.9, 144.9, 154.9,

161.2 and 165.8; HRMS (ESI+): calc. for $C_{22}H_{28}N_3O_4S_2$ $[M+H]^+$ 426.1521, found: 462.1523.

Anal. calc. for $C_{22}H_{27}N_3O_4S_2$: C 56.8, H 6.6, N 8.3, found: C 56.7 H 6.4, N 8.1.

2-(1-Hydroxyethyl)deazathiamin   diphosphate   (15).   *Tris*(tetrabutylammonium)

pyrophosphate (544 mg, 0.60 mmol) was added portionwise to a stirred solution of **25**

(140 mg, 0.30 mmol) in dry acetonitrile (0.6 mL) under an inert atmosphere. The reaction

mixture was stirred at 4 ºC for 8 h before being diluted with milliQ water (1.0 mL). The

solution was purified by ion-exchange chromatography using a Sephacel DEAE column

eluting with a gradient of 0 to 0.25 M aq. NH_4HCO_3. Concentration by lyophilization gave

pyrophosphate **15** as a white powder (76 mg, 61%). δ_H (500 MHz, D_2O) 1.40 (3 H, d, J =

6.4), 1.87 (3 H, s), 2.36 (3 H, s), 3.06 (2 H, t, J = 6.7), 3.60 (2 H, s), 4.03 (2 H, app. q, J =

6.7), 5.04 (1 H, q, J = 6.4) and 7.18 (1 H, s), protons of amino group and hydroxyl group not

visible. δ_C (125 MHz, D_2O) 11.8, 22.8, 24.6, 24.9, 29.3, 64.1, 66.3, 114.3, 131.8, 133.4,

134.9, 142.5, 148.5, 162.9 and 163.8. δ_P (162 MHz, D_2O) −5.93 and −9.90 (2 x 1 P, d, J 21.5,

O*POPO*). HRMS (ESI–): calc. for $C_{15}H_{23}N_3O_8SP_2$ $[M]^-$ 467.0681, found: 467.0690. The

batch of **15** tested in this work was a mixture with ammonium tosylate (1:1 molar ratio).

Computational Methods

M. tuberculosis **DXS Model-Building**

All calculations were performed within the Discovery Studio 2.5.5 suite of protocols (Accelrys

Inc., San Diego, CA) and Maestro 9.0.211 (Schrödinger, LLC, New York, NY). Computations

were run on a quad core Intel 3.0 GHz Xeon processor X5472.

Protein-BLAST search at NCBI (http://blast.ncbi.nlm.nih.gov/Blast.cgi) was employed in order to identify the most suitable template(s) for model building. The BLAST-P search algorithm identified the *D. radiodurans* DXS (PDB code 2O1X) structure as the best. There is a 37.9% identity and 57.4% similarity between the two sequences based on the 'align sequences' protocol within Discovery Studio.

The *M. tuberculosis* DXS homology model was generated using the comparative modeling program MODELLER.[38,39] There is a stretch of residues that is missing in the *D. radiodurans* DXS structure. Thus, three approaches were undertaken in order to build the model and eventually select the most physically plausible structure. Specifically: 1) The loop in *M. tuberculosis* DXS that corresponds to the missing residues was eliminated, followed by a break insertion in both template and model sequences; 2) A model structure was generated with the loop corresponding to the missing residues of 2O1X constructed *de novo*, that is no breaks were inserted; and 3) Three alternative templates (PDB codes 3EXC, 1HJS, and 3MQO) were employed in order to build the missing loop. In all model-building experiments, structures were generated with the ligand in 2O1X being copied (routine 'copy from templates' and 'ligands' within the MODELER protocol) to the newly constructed models. It should be pointed out that five models were generated in each run, and the optimization level was set to high. All models were constructed with the loop refinement option turned on at medium optimization level, and the Discrete Optimized Protein Energy (DOPE)[3b] potential for scoring (both raw and normalized DOPE were used).

The final models were refined using limited minimization. Constraints on the backbone were imposed, and the CHARMM force field was employed, while the Momany Rone[40] method was used for partial charges. Initial minimization was performed with 500 steps of steepest descent

and a convergence criterion of the gradient set at 0.1, followed by 1500 steps of conjugate gradient and convergence of 0.0001.

The quality of the constructed models was assessed using the DOPE scoring function and the Verify Protein (Profile 3D) protocol, as implemented in Discovery Studio. DOPE measures the relative stability of one conformation compared to all other generated conformations for the same protein. The raw DOPE score has an arbitrary scale, and thus it is not normalized on protein size; nevertheless, it can still be used when comparing proteins with the same sequences. The normalized DOPE is a Z-score derived from the statistics of raw DOPE scores from a database of models. A lower DOPE score is indicative of smaller errors in the mode, while a normalized DOPE scores lower than −1 are likely to be native-like. Profiles-3D reduces the 3D structures to a 1D string of residue environments, which, in turn, can be used to check the validity of the generated models by measuring their compatibility with the primary sequence. PROCHECK was employed in order to assess the stereochemical quality of the model-built structures. No manual modification of the phi-psi angles of amino acids that fell into the unacceptable quadrant was undertaken as they were few and away from the region of interest.

Ligand Docking

Because our intent was to understand differential binding, docking was performed in both the crystal *D. radiodurans* DXS and model-built *M. tuberculosis* DXS structures. Glide 5.5 within Maestro 9.0 (Schrodinger, LLC: New York, NY) was employed for all docking experiments. Structures of the docked compounds are shown in Table 3. Prior to docking, the receptor was prepared by assigning bond orders, adding hydrogen atoms and finding overlaps, followed by hydrogen-bond optimization and minimization using the Protein Preparation Wizard.

Minimization employed the 'Impref' utility, which runs a series of constrained impact minimizations with gradually decreasing strength of the heavy-atom restraining potential. Specifically, two minimizations are initially performed with the heavy-atom restraint potential force constant at 10. In the first minimization, the torsional potential is turned off to improve hydrogen optimization, whereas the second minimization restores the torsional potential. The restraining potential force constant is subsequently reduced to 3, 1, 0.3, and 0.1. If the output structure from a minimization exceeds the specified RMSD threshold, relative to the starting structure, the program stops and returns the structure from the previous minimization. Thus, the RMSD is checked at the end of each round of minimization. Receptor-grid generation was subsequently employed with the van der Waals radius scaling factor set to 1.0, and partial charge cut-off at 0.25. The binding pocket for *D. radiodurans* DXS was defined within 10 Å from the bound ligand, while in *M. tuberculosis* DXS the pocket was encompassed by Glu 365, Phe 390, Ser 112, Ala 114, His 71, Asn 173, Arg 175, and Asp 144. Standard Precision was employed for all docking calculations with ten poses per ligand and post-docking minimization. Poses were selected using experimental data as guides and the number of feasible bonding interactions.

Biological Evaluation. Gene Expression and Protein Purification. IC$_{50}$ Determination Using the Photometric Assay *D. radiodurans* DXS and *M. tuberculosis* DXS were expressed and purified according to a protocol reported in the literature.[10] The biochemical assay for the determination of the inhibitory activity of the ThDP-derivatives against *D. radiodurans* DXS and *M. tuberculosis* DXS has been performed as described by us in a previous publication.[10]

References

[1] (a) World Health Organization, Global Tuberculosis Report 2014, ISBN 978 92 4 156480 9, (b) World Health Organization, World Malaria Report 2014, ISBN: 978 92 4 156483 0.

[2] (a) C. Wongsrichanalai, J. K. Varma, J. J. Juliano, M. E. Kimerling and J. R. MacArthur, *Emerg. Infect. Dis.*, 2010, **16**, 1063−1067, (b) N. R. Gandhi, P. Nunn, K. Dheda, H. S. Schaaf, M. Zignol, D. van Soolingen, P. Jensen and J. Bayona, *Lancet*, 2010, **375**, 1830−1840, (c) C. Cotter, H. J. W. Sturrock, M. S. Hsiang, J. Liu, A. A. Phillips, J. Hwang, C. S. Gueye, N. Fullman, R. D. Gosling and R. G. A. Feachem, *Lancet*, 2013, **382**, 900−911.

[3] (a) M. Rohmer, M. Seemann, S. Horbach, S. Bringer-Meyer and H. Sahm, *J. Am. Chem. Soc.*, 1996, **118**, 2564–2566; (b) M. Rohmer, *Nat. Prod. Rep.*, 1996, **16**, 565–574; (c) D. Arigoni, S. Sagner, C. Latzel, W. Eisenreich, A. Bacher and M. H. Zenk, *Proc. Natl. Acad. Sci. U. S. A.*, 1997, **94**, 10600–10605; (d) W. N. Hunter, *J. Biol. Chem.*, 2007, **282**, 21573–21577.

[4] (a) J.-Y. van der Meer and A. K. H. Hirsch, *Nat. Prod. Rep.*, 2012, **29**, 721−728; (b) I. Hale, P. M. O'Neill, N. G. Berry, A. Odom and R. Sharma, *MedChemComm*, 2012, **3**, 418−433; (c) T. Masini, B. S. Kroezen and A. K. H. Hirsch, *Drug Discov. Today*, 2013, **18**, 1256−1262; (d) T. Masini and A. K. H. Hirsch, *J. Med. Chem.*, 2014, **57**, 9740−9763.

[5] (a) G. A. Sprenger, U. Schörken, T. Wiegert, S. Grolle, A. A. deGraaf, S. V. Taylor, T. P. Begley, S. Bringer-Meyer and H. Sahm, *Proc. Natl. Acad. Sci. U. S. A.*, 1997, **94**, 12857–12862; (b) B. M. Lange, M. R. Wildung, D. McCaskill and R. A. Croteau, *Proc. Natl. Acad. Sci. U. S. A.*, 1998, **95**, 2100–2104; (c) P. Léon and E. Cordoba, in *Isoprenoid synthesis in plants and microorganisms: new concepts and experimental approaches*"; Bach, T. J., Rohmer, M. Eds

Springer New Tork, 2013, p. 459; (d) A. C. Brown, M. Eberl, D. C. Crick, H. Jomaa and T. Parish, *J. Bacteriol.*, 2010, **192**, 2424–2433.

[6] V. K. Singh and I. Ghosh, *FEBS Lett.*, 2013, **587**, 2806−2817.

[7] Q. Du, H. Wang and J. Xie, *Int. J. Biol. Sci.*, 2011, **7**, 41−52.

[8] R. E. Hill, K. Himmeldirk, I. A. Kennedy, R. M. Pauloski, B. G. Sayer, E. Wolf and I. D. Spenser, *J. Biol. Chem.*, 1996, **271**, 30426−30435.

[9] S. Xiang, G. Usunow, G. Lange, M. Busch and L. Tong, *J. Biol. Chem.*, 2007, **282**, 2676−2682.

[10] T. Masini, J. Pilger, B. S. Kroezen, B. Illarionov, P. Lottmann, M. Fischer, C. Griesinger and A. K. H. Hirsch, *Chem. Sci.*, 2014, **5**, 3543–3551.

[11] E. Fiedler, S. Thorell, T. Sandalova, R. Golbik, S. Konig and G. J. Schneider, *Mol. Biol.*, 1995, **238**, 387–404.

[12] P. Arjunan, N. Nemeria, A. Brunskill, K. Chandrasekhar, M. Sax, Y. Yan, F. Jordan, J. R. Guest and W. Furey, *Biochemistry*, 2002, **41**, 5213–5221.

[13] R. A. Frank, F. J. Leeper and B. F. Luisi, *Cell. Mol. Life Sci.*, 2007, **64**, 892–905.

[14] F. Morris, R. Vierling, L. Boucher, J. Bosch and C. L. Freel Meyers, *ChemBioChem*, 2013, **14**, 1309–1315.

[15] (a) L. M. Eubanks and C. D. R. Poulter, *Biochemistry*, 2003, **42**, 1140–1149; (b) H. Patel, N. S. Nemeria, L. A. Brammer, C. L. Freel Meyers and F. Jordan, *J. Am. Chem. Soc.,* 2012, **134**, 18374–18379; (c) L. A. Brammer, J. M. Smith, H. Wade and C. L. Freel Meyers, *J. Biol. Chem.*, 2011, **286**, 36522–36531.

[16] R. Kluger and K. Tittmann, *Chem. Rev.*, 2008, **108**, 1797–1833.

[17] (a) J. Mao, H. Eoh, R. He, Y. Wang, B. Wan, S. G. Franzblau, D. C. Crick and A. P. Kozikowski, *Bioorg. Med. Chem. Lett.*, 2008, **18**, 5320−5323; (b) D. Hayashi, N. Kato, T. Kuzuyama, Y. Satoc, J. Ohkanda, *Chem. Commun.*, 2013, **49**, 5535–5537.

[18] (a) J. M. Smith, R. J. Vierling and C. L. Freel Meyers, *MedChemComm*, 2012, **3**, 65−67; (b) J. M. Smith, N. V. Warrington, R. J. Vierling, M. L. Kuhn, W. F. Anderson, A. T. Koppisch and C. L. Freel Meyers, *J. Antibiot.*, 2014, **67**, 77−83.

[19] (a) J. Querol, M. Rodríguez-Concepción, A. Boronat and S. Imperial, *Biochem. Biophys. Res. Commun.*, 2001, **289**, 155–160; (b) M. Nikkola, Y. Lindqvist and G. Schneider, *J. Mol. Biol.*, 2004, **238**, 387–404.

[20] S. Sauret-Güeto, E. M. Urós, E. Ibáñez, A. Boronat and M. A. Rodríguez-Concepción, *FEBS Lett.*, 2006, **580**, 736–740.

[21] K. Agyei-Owusu and F. J. Leeper, *FEBS Journal*, 2009, **276**, 2905–2916.

[22] S. Mann, C. P. Melero, D. Hawksley, F. J. Leeper, *Org. Biomol Chem*, 2004, **2**, 1732–1741.

[23] C. L. Berthold, D. Gocke, M. D. Wood, F. J. Leeper, M. Pohl and G. Schneide, *Acta Crystallogr.*, 2007, **63**, 1217–1224.

[24] T. S. Elliott, A. Slowey, Y. Ye and S. J. Conway, *Med. Chem. Commun.*, 2012, **3**, 735−751.

[25] (a) K. M. Erixon, C. L. Dabalos and F. J. Leeper, *Chem. Commun.*, 2007, 960–962; (b) J. He, L. Feng, J. Li, R. Tao, F. Wang, X. Liao, Q. Sun, Q. Long, Y. Ren, J. Wan, J. and H. He, *Bioorg. Med. Chem.*, 2012, **20**, 1665–1670.

[26] A. A. Thomas, J. De Meese, Y. Le Huerou, S. A. Boyd, T. T. Romoff, S. S. Gonzales, I. Gunawardana, T. Kaplan, F. Sullivan, K. Condroski, J. P. Lyssikatos, T. D. Aicher, J. Ballard, B. Bernat, W. DeWolf, M. Han, C. Lemieux, D. Smith, S. Weiler, S. K. Wright, G. Vigers and B. Brandhuber, *Bioorg. Med. Chem. Lett.*, 2008, **18**, 509−512.

[27] (a) J. D. Thompson, D. G. Higgins and T. J. Gibson, *Nucleic Acids Res.,* 1994, **22**, 4673−4680; (b) S. F. Altschul, W. Gish, W. Miller, E. W. Myers and D. J. Lipman, *J. Mol. Biol.,* 1990, **215**, 403−410; (c) S. F. Altschul and D. J. Lipman, *Proc. Natl. Acad. Sci. U S A,* 1990, **87**, 5509−5513; (d) W. Gish and D. J. States, *Nat. Genet., 1*993, **3**, 266−272; (e) T. L. Madden, R. L. Tatusov and J. Zhang, *Methods Enzymol,* 1996, **266**, 131−141; (f) J. Zhang and T. L. Madden, *Genome Res.,* 1997, **7**, 649−656.

[28] M. Y. Shen and A. Sali, *Protein Sci.,* 2006, **15**, 2507−2524.

[29] R. Luthy, J U. Bowie, D. Eisenberg, *Nature,* 1992, **356**, 83−85.

[30] H. Zhao, L. P. S. de Carvalho, C. Nathan and O. Ouerfelli, *Bioorg. Med. Chem. Lett.*, 2010, **20**, 6472−6474.

[31] L. J. Y. M. Swier, L. Monjas, A. Guskov, A. R. de Voogd, G. B. Erkens, D. J. Slotboom and A. K. H. Hirsch, *ChemBioChem*, 2015, **16**, 819−826.

[32] P. R. Gerber and K. Müller, *J. Comput.-Aided Mol. Des.*, 1995, **9**, 251−268.

[33] P. Kuzmic, *Anal. Biochem.* 1996, **237**, 260−273.

[34] V. M. Sanchez-Pedregal, M. Reese, J. Meiler, M. J. J. Blommers, C. Griesinger and T. Carlomagno, *Angew. Chem. Int. Ed.*, 2005, **44**, 4172−4175.

[35] (a) R. A. Friesner, J. L. Banks, R. B. Murphy, T. A. Halgren, J. J. Klicic, D. T. Mainz, M. P. Repasky, E. H. Knoll, M. Shelley, J. K. Perry, D. E. Shaw, P. Francis and P. S. Shenkin, *J. Med. Chem.* 2004, **47**, 1739−1749; (b) R. A. Friesner, R. B. Murphy, M. P. Repasky, L. L. Frye, J. R. Greenwood, T. A. Halgren, P. C. Sanschagrin and D. T. Mainz, *J. Med. Chem.,* 2006, **49**, 6177−6196; (c) T. A. Halgren, R. B. Murphy, R. A. Friesner, H. S. Beard, L. L. Frye, W. T. Pollard and J. L. Banks, *J. Med. Chem.,* 2004, **47**, 1750−1759.

[36] (a) M. Kontoyianni, L. M. McClellan and G. S. Sokol, *J. Med. Chem.,* 2004, **47**, 558–565; (b) M. Kontoyianni, G. S. Sokol and L. M. McClellan, *J. Comput. Chem.,* 2005, **26**, 11–22; (c) G. L. Warren, C. W. Andrews, A. M. Capelli, B. Clarke, J. LaLonde, M. H. Lambert, M. Lindvall, N. Nevins, S. F. Semus, S. Senger, G. Tedesco, I. D. Wall, J. M. Woolven, C. E. Peishoff and M. S. Head, *J. Med. Chem.,* 2006, **49**, 5912–5931; (d) M. D. Cummings, R. L. DesJarlais, A. C. Gibbs, V. Mohan and E. P. Jaeger, *J. Med. Chem.,* 2005, **48**, 962–976.

[37] S. Lüdtke, P. Neumann, K. M. Erixon, F. J. Leeper, R. Kluger, R. Ficner and K. Tittmann, *Nature Chem.,* 2013, **5**, 762–767.

[38] A. Sali and T. L. Blundell, *J. Mol. Biol.,* 1993, **234**, 779–815.

[39] M. A. Marti-Renom, A. C. Stuart, A. Fiser, R. Sanchez, F. Melo, A. Sali, *Annu. Rev. Biophys. Biomol. Struct.,* 2000, **29**, 291–325.

[40] F. A. Momany and R. Rone, *J. Comput. Chem.*, 1992, **13**, 888–900.